A semi-automated segmentation framework for MRI based brain tumor segmentation using regularized nonnegative matrix factorization

Nicolas Sauwen*,†, Diana M Sima*,†, Marjan Acou‡, Eric Achten‡, Frederik Maes*, Uwe Himmelreich§ and Sabine Van Huffel*,†
*Department of Electrical Engineering (ESAT), KU Leuven, Leuven, Belgium
Email: nicolas.sauwen@kuleuven.be
†Department Medical Information Technologies, iMinds, Belgium
‡Department of Radiology, Ghent University Hospital, Ghent, Belgium
§Department of Imaging and Pathology, Biomedical MRI/MoSAIC, KU Leuven, Leuven, Belgium

***Abstract*—Segmentation plays an important role in the clinical management of brain tumors. Clinical practice would benefit from accurate and automated volumetric delineation of the tumor and its subcompartments. We present a semi-automated framework for brain tumor segmentation based on regularized nonnegative matrix factorization (NMF). L1-regularization is incorporated into the NMF objective function to promote spatial consistency and sparseness of the tissue abundance maps. The pathological sources are initialized through user-defined voxel selection. Knowledge about the spatial location of the selected voxels is combined with tissue adjacency constraints in a post-processing step to enhance segmentation quality. The method is applied to the BRATS 2013 Leaderboard dataset, consisting of publicly available multi-sequence MRI data of brain tumor patients. Our method performs well in comparison with state-of-the-art, in particular for the enhancing tumor region, for which we reach the highest Dice score among all participants.**

***Keywords*-Magnetic resonance imaging; brain tumor; segmentation; nonnegative matrix factorization**

I. Introduction

Tumor segmentation plays an important role in treatment planning as well as during follow-up of brain tumors. Criteria to assess response to treatment in brain tumors have recently been updated by the response assessment in neuro-oncology (RANO) working group [1]. Following these criteria, growth or shrinkage of the lesion is evaluated by measuring the maximal diameters of the lesion in 2 orthogonal directions. The RANO group has acknowledged that volumetric measurements might be favourable compared to cross-product diameters in the case of irregularly shaped tumors, multi-focal tumors and tumors with cystic or necrotic components. Furthermore, several studies have shown that volumetric measures of the tumor subcompartments carry prognostic information [2], [3]. These findings suggest that inclusion of volumetric measures of the tumor subcompartments might improve prediction of individual patient survival.

Segmentation of brain tumors is a challenging task. Gliomas, which represent the most common type of primary brain tumor [4], are known to be highly heterogeneous. Several stages of the disease can occur within the same lesion and boundaries between pathological tissue regions are diffuse. Magnetic resonance imaging (MRI) has become the imaging modality of choice in the management of brain tumor patients. As several types of MRI images have to be combined in order to differentiate the tumor subcompartments, lack of co-registration between the images further complicates the segmentation process. Manual segmentation is currently the gold standard, but it is a tedious and time-consuming task.

In recent years, significant advancements have been made in the field of automated brain

tumor segmentation. Both semi-automated and fully automated methods have been proposed [5]. A popular approach is to combine imaging biomarkers from different MRI sequences on a voxel-wise basis, to increase specificity and reduce overlap between the tissue classes. Nowadays, supervised classification methods have been receiving most attention [6]. These methods rely on an extensive set of training images with manually annotated ground truth to learn decision boundaries between the tissue classes in feature space. The most popular methods include random forests [7], support vector machines [8] and neural networks [9]. Unsupervised classification methods, on the other hand, are very flexible, as they don't require an extensive training dataset with a uniform acquisition protocol. They learn classification rules directly from the imaging data at hand, based on some similarity criterion. Popular approaches include fuzzy C-means clustering [10], Gaussian mixture modeling [11], hidden Markov Random Fields [12] and nonnegative matrix factorization [13]. Since they do not use training data, unsupervised methods rely more strongly on the incorporation of prior knowledge to obtain competitive results.

Due to the lack of a publicly available brain tumor MRI database with ground-truth segmentations, so far most segmentation studies have evaluated their algorithms on relatively small private datasets. This has complicated comparison of the performance of different methods against each other in an unbiased way. Recently, the Multimodal Brain Tumor Segmentation (BRATS) challenge has made available an open database of brain tumor images, serving as a benchmark for objectively comparing segmentation algorithms [6]. A unique dataset of MR scans of both low- and high-grade glioma patients is provided. A training dataset with known ground-truth is made available, which can be used by different groups to tune their algorithms. Evaluation of the segmentation methods is then based on a test dataset, for which the ground-truth is not made publicly available. In this way, results are not influenced by overtraining of the method being tested.

This paper presents a semi-automated tumor segmentation method based on regularized nonnegative matrix factorization (NMF). User-defined seeding points in the pathological regions are combined with a sophisticated seeding method for the normal brain tissues to initialize the NMF algorithm. Piece-wise spatial smoothness as well as sparseness of the NMF tissue abundance maps are encouraged through L1-regularization. Morphological post-processing based on the spatial location of the user-defined seeds is exploited to further remove false positives. The method will be applied to the BRATS 2013 Leaderboard dataset. Segmentation results are compared against the algorithms submitted to the BRATS 2013 challenge as reported in [6].

II. BRATS 2013 Leaderboard dataset

The BRATS 2013 Leaderboard dataset consists of multi-contrast MRI scans of 21 high-grade glioma and 4 low-grade glioma patients. The images were acquired at different hospitals over the course of several years, using MR scanners from different vendors and with different field strengths. For each patient, T_1-weighted, T_2-weighted, fluid-attenuated inversion recovery (FLAIR) and post-contrast T_1-weighted (T1c) images were provided. All images were skull-stripped, rigidly co-registered to the T1c sequence and resampled to $1mm^3$ isotropic resolution. The following tissue classes were differentiated by expert annotation: necrosis, edema, non-enhancing tumor and enhancing tumor.

III. Methodology

A. Bias field correction

Intensity inhomogeneity is a common artefact in MRI images. These magnetic field inhomogeneities, also known as bias fields, consist of low-frequency intensity variations that corrupt the images. As most automated segmentation algorithms assume the same intensity level throughout the same tissue class, bias fields must be corrected for to ensure proper segmentation. Various bias field correction algorithms have been proposed, but the non-parametric

non-uniform normalization (N3) approach formulated in [14] has established itself as a reference method. We used the N4 method, a recently proposed new implementation of N3, with a better B-spline fitting function and a hierarchical optimization scheme for the bias field correction [15].

B. Nonnegative matrix factorization

NMF decomposes a nonnegative input matrix X into the product of 2 low-rank nonnegative factor matrices W and H, imposing nonnegativity to all the elements:

$$\begin{aligned} X \approx WH \quad &\text{with} \quad X \in R_+^{m\times n}, \\ W \in R_+^{m\times r} \quad &\text{and} \quad H \in R_+^{r\times n} \end{aligned} \tag{1}$$

The n columns of X represent the data points, each of which contains m features. NMF approximates each data point as a weighted sum of r source vectors. The source vectors are the columns of W and the weights (or abundances) per data point are the columns of H. In the context of tumor segmentation, each voxel corresponds to one data point and the MR image intensities are the features. Each voxel's feature vector will be modeled as a weighted sum of the r sources in W. The sources are expected to represent the different tissue types, so each source contains a tissue-specific signature. One row of H contains the weights for one tissue type over all the voxels. Such a row can be spatially transformed back to the imaging domain, to obtain tissue-specific abundance maps. The most commonly used similarity metric to quantify the difference between X and its NMF approximation WH is based on the squared Euclidean distance:

$$\begin{aligned} &\min_{W,H} f(W,H) = \min_{W,H} \quad \frac{1}{2}\|X - WH\|_F^2 \\ &\forall i,j : W_{i,j} \geq 0, \quad H_{i,j} \geq 0 \end{aligned} \tag{2}$$

Structured data fusion NMF (SDF NMF) is being used as implemented in Tensorlab [16]. A transformation of variables is used to convert the constrained optimization problem in Equation 2 into an unconstrained problem, by squaring the entries of the factor matrices. The Gauss-Newton algorithm with dogleg trust region is used to solve the resulting non-linear least-squares problem. The SDF framework allows straightforward incorporation of regularization terms into the objective function. An L1-regularization term was included to promote both spatial consistency as well as sparseness of the tissue abundance maps:

$$\begin{aligned} \min_{W,H} f(W,H) = \min_{W,H} \quad &\frac{1}{2}(\|X - WH\|_F^2 \\ &+\lambda\|(L+I)H\|_1) \end{aligned} \tag{3}$$

The L1-regularization term in Equation 3 in fact consists of 2 terms. The first term, LH, promotes piece-wise smoothness on the abundance maps. L is a sparse $n\times n$ matrix, with each row containing a vectorized Laplacian kernel. Each row of L applies a two-dimensional second order spatial derivative to the corresponding voxel. An in-plane neighborhood of 4 voxels is considered for the Laplacian kernel. The second term applies L1-regularization to H directly, imposing sparseness to the abundance maps. The regularization coefficient λ was empirically set to 0.1. To reduce computation time, NMF analyses were limited to a manually selected slice range comprising the pathological region. Also, a downsampling factor of 2 was applied along the x- and y-axes of each image slice.

C. NMF initialization

As NMF poses a non-convex optimization problem, initialization of the factor matrices (W_0 and H_0) is required. The pathological tissue sources are initialized based on voxel selection. The user is required to select one or more voxels in each pathological region, i.e. active tumor and, if present, necrosis and edema. For each selected voxel, a candidate source vector is added to W_0 as the averaged feature vector of the selected voxel and its 4 in-plane neighboring voxels. For each pathological tissue class, we then calculate the correlation coefficient between the candidate source vectors as their inner vector product after normalization. The initial pathological sources are obtained after merging candidate source vectors with a correlation coefficient higher than 0.95 in W_0 and replacing them by

their average, thereby reducing complexity of the NMF model.

As the normal brain tissue types (i.e. white matter, gray matter, cerebro-spinal fluid and blood vessels) are still highly abundant in the affected brain, an automated seeding procedure is used to obtain their initial source vectors. To cope with the variance within the tissue classes, 2 sources are assigned to each normal tissue type, leading to a total of 8 normal tissue sources. We use the successive projection algorithm (SPA) [17] to obtain an initial estimate of the normal sources. SPA returns a subset of voxels from the input matrix X with minimal collinearity in feature space. Similarly to the pathological sources, the normal sources are obtained as the averaged feature vector of each selected voxel and its 4 in-plane neighboring voxels. As SPA is known to be sensitive to outliers, an additional fuzzy C-means (FCM) procedure is applied, using the initial pathological sources and the normal sources obtained from SPA to initialize the cluster centroids. As we already obtained proper initialization of the pathological tissue types through user input, the pathological cluster centroids are forced to remain the same throughout the FCM updating procedure. The final FCM centroids make up the columns of W_0. The columns of H_0 are found by applying non-negative least squares fitting to the columns of X and W_0.

To initialize the pathological sources, an experienced radiologist (MA, UZ Gent) selected voxels in the tumor subcompartments of each patient. Between 3 and 5 voxels were selected by the radiologist in each subcompartment. To be able to quantify intra-user variability of the segmentation results, the radiologist was asked to repeat voxel selection on the same patients 2 more times. An interval of at least 24 hours was admitted between subsequent voxel selection on the same patient.

D. Morphological post-processing

After NMF analysis, each voxel is assigned to the source for which it has the highest abundance value. Voxels that were assigned to different sources belonging to the same pathological tissue class are merged to obtain a preliminary tissue segmentation mask. A morphological post-processing procedure, consisting of 2 steps is then applied to the pathological segmentation masks to remove false positives. Spatial consistency of the tissue regions is assumed, therefore the segmentation masks are analysed in terms of (3D-)connected components. For each pathological tissue type, only the connected components containing at least one user-defined voxel are withheld in the tissue segmentation masks (Step 1). To avoid missing disjoint regions of a tumor component for which no voxels were selected by the user, an additional step is performed which assumes spatial connectivity of the various pathological components (Step 2). Necrotic areas are always adjacent to an active tumor region. Therefore, any connected component of the preliminary necrosis mask which has a common edge with any withheld active tumor component is also included. Similarly, components of the preliminary active tumor mask are also included if they have a common edge with any withheld necrotic component. The same procedure is also applied to edema, by verifying spatial adjacency to the active tumor region(s).

E. Validation

The BRATS challenge reports validation scores for the following tissue classes: enhancing tumor, the tumor core (i.e. enhancing tumor, non-enhancing tumor and necrosis) and the whole tumor (i.e. the tumor core and edema). Dice score [6], positive predictive values (PPV) and sensitivity values are reported to evaluate segmentation overlap.

IV. Results

Figure 1 shows the segmentation of the tumor subcompartments of a high-grade glioma patient using L1-regularized NMF. Some false positive regions of edema were segmented in gray matter areas of the frontal cortex.

Table I compares the performance of L1-regularized NMF-based segmentation (Sauwen) to the best performing methods from the BRATS 2013 challenge, as well some other methods reported in literature. As we repeated NMF analyses 3 times on each patient using

different voxel selection, averaged results over the 3 runs are reported. The 5 best performing methods of the BRATS challenge (Tustison, Zhao, Meier, Reza and Cordier) all used fully automated methods based on supervised classification [6]. So far, the best results reported in literature on the Leaderboard dataset are based on the method by Kwon *et al.* [18]. They combine a healthy brain atlas with a tumor growth model, using seeding points selected by the user to initialize tumor growth. The tissue priors obtained from this model are then fed into a Gaussian mixture model (GMM) along with the MRI features to obtain the final segmentation. Competitive results were also reported by Juan-Albarracin *et al.* [11]. They also applied GMM to a set of MRI features including intensity values and texture features, then used a healthy brain atlas to distinguish the actual pathological components.

As can be seen from Table I, competitive segmentation results are obtained using L1-regularized NMF. Looking at the enhancing tumor region, our method reaches a mean Dice score of 0.64, which is the highest Dice score among all considered methods. For the tumor core, we obtain a Dice score of 0.64, which is also among the best performing methods for this tissue class. For the whole tumor region, a Dice score of 0.72 is found, which is rather low as all other methods except for Meier obtain higher Dice scores. Also when looking at the PPV and sensitivity values, it can be seen that L1-regularized NMF is one of the best methods for the enhancing tumor region, scores quite well for the tumor core but relatively low for the whole tumor region.

To assess robustness of the segmentation results against user input variability, Fig. 2 shows the Dice score ranges per patient over the 3 repeated runs with different voxel selection. In about half of the cases, the Dice score did not vary by more than 5% over the different runs. 75% of the Dice score ranges were below 10%, and 86% of the Dice scores varied by no more than 15%. Higher Dice score variations were mainly attributable to 3 patients (patients 1, 6 and 11), exhibiting Dice score ranges larger than 15% for each tissue class. When considering mean Dice score variations at the group level, differences were not higher than 3% for any tissue class.

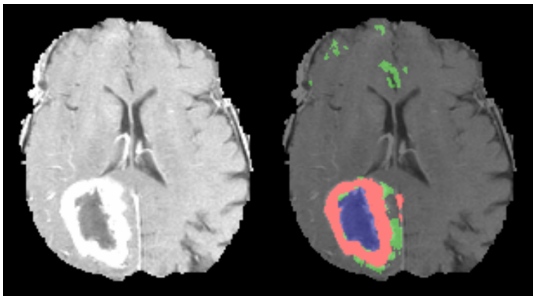

Figure 1. Axial T1c slice of a high-grade glioma patient, and the segmentation of the tumor subcompartments using L1-regularized NMF (red=enhancing tumor, blue=necrosis, green=edema).

V. Discussion

Although the vast majority of segmentation algorithms participating in the BRATS 2013 challenge were based on supervised classifiers, it has been shown in this paper that unsupervised classifiers incorporating adequate prior knowledge can be highly competitive. In fact, the best segmentation results that have so far been reported on the BRATS 2013 Leaderboard dataset were obtained by Kwon *et al.*, combining tissue prior probabilities obtained from a tumor growth model with GMM [18]. Besides non-rigid coregistration to a healthy brain atlas on which the tumor growth model is based, additional prior knowledge in the form of user input was included: user-defined seeding points were used along with an approximate radius estimation of the lesion(s) to initialize tumor class parameters. Competitive segmentation results were also obtained using L1-regularized NMF. A mean Dice score of 0.64 was found for the enhancing tumor region. To our knowledge, no method reported in literature has so far reached such a high mean Dice score for enhancing tumor on the Leaderboard dataset. With a mean Dice score of 0.64, L1-regularized NMF also ranks among the better methods for the tumor core. For the whole tumor region, a mean Dice score of 0.72 was found, which is relatively low compared to

Table I
MEAN DICE SCORE, PPV AND SENSITIVITY VALUES OF THE ENHANCING TUMOR, TUMOR CORE AND WHOLE TUMOR REGION ON THE BRATS 2013 LEADERBOARD DATASET.

	Dice			PPV			Sensitivity		
	Enhancing	Core	Whole	Enhancing	Core	Whole	Enhancing	Core	Whole
Tustison [6]	0.53	0.65	0.79	0.51	0.70	0.83	**0.66**	0.73	0.81
Zhao [6]	0.47	0.59	0.79	0.50	0.55	0.77	0.53	0.77	0.85
Meier [6]	0.53	0.60	0.72	0.48	0.62	0.65	0.64	0.69	**0.88**
Reza [6]	0.51	0.56	0.73	0.48	0.64	0.68	0.63	0.57	0.79
Cordier [6]	0.46	0.61	0.75	0.43	0.61	0.79	0.52	0.72	0.78
Sauwen	**0.64**	0.64	0.72	**0.71**	0.71	0.78	0.65	0.69	0.72
Kwon [18]	0.59	**0.79**	**0.86**	0.60	**0.84**	**0.88**	0.63	**0.81**	0.86
Albarracin [11]	0.60	0.59	0.74	0.60	0.55	0.71	**0.66**	0.71	0.81

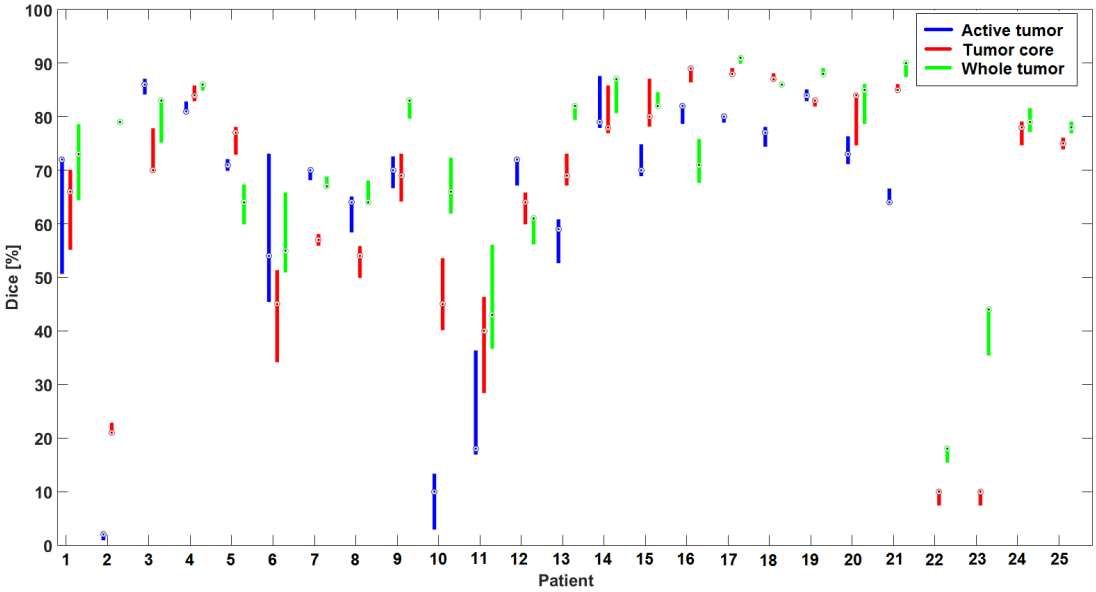

Figure 2. Dice score ranges per patient over 3 repeated runs with different voxel selection.

the other algorithms: several groups reached Dice scores close to 0.80 or even higher. One of the main reasons for this fallback is the relatively high amount of false positives for edema. Mainly, gray matter voxels exhibited feature vectors similar to edema. Gray matter structures were sometimes wrongfully annotated as edema and could not properly be removed using morphological post-processing when connected with the true edema region. Additional incorporation of prior knowledge will probably allow further improvement of the segmentation results.

Computation time of the L1-regularized NMF algorithm per patient depended on the slice range to be analysed and the rate of convergence. On average, a computation time of about 75 minutes was found. For the BRATS 2013 challenge, reported computation times varied considerably among participants, with some algorithms taking a few minutes per patient while others required more than one hour [6], like our method. Although the treatment of brain tumors does not require immediate

feedback for clinical intervention, computation times of one hour or more are inconvenient, and might not be accepted in clinical practice. The NMF computation itself takes up most of the time. More efficient NMF algorithms do exist and might have to be considered to bring down computation time. There were mainly 2 reasons why SDF NMF was used in the current work. First of all, SDF NMF allows the incorporation of L1-regularization into the objective function. Other NMF implementations such as HALS NMF or Convex NMF do not straightforwardly incorporate L1-regularization, as it renders the NMF objective function non-differentiable. Secondly, SDF NMF is sensitive to the initialization of the factor matrices. Whereas insensitivity to initialization might be an asset in the case of suboptimal initialization, in the current work it is known that initial estimates of the pathological sources are already quite accurate, as they are based on user input. To reduce computation time, in-plane downsampling of the images was applied with a factor 2 in both slice directions. Out-of-plane downsampling is not implemented, as often MRI voxels are anisotropic, with relatively low out-of-plane resolution. In case of the BRATS data, however, interpolated voxels had an isotropic resolution of $1mm^3$. As such, computation times can be further reduced by also allowing out-of-plane downsampling. One might explore whether relaxation of the NMF convergence criteria could further reduce computation time, while maintaining segmentation performance.

Robustness against user input variability is an important requirement that needs to be fulfilled by semi-automated methods. Intra-user variability of semi-automated NMF was verified by repeating analyses 3 times with different voxel selection by the same radiologist. Variation of the Dice score per patient and per tissue class was found to be within 10% in 75% of the cases and within 15% in 86% of the cases. Mainly for 3 patients, 1 out 3 runs gave Dice scores for all tissue classes that were considerably lower, decreasing by close to 20% or more, compared to the other 2 runs. Mazzara *et al.* have reported an average intra-rater variability of $20 \pm 15\%$ for the manual segmentation of brain tumor volumes [19]. Therefore, a certain degree of segmentation variability is unavoidable. Nevertheless, further development of semi-automated NMF-based segmentation should not only focus on higher performance but also on increased robustness of the results.

VI. Conclusion

In this paper, semi-automated segmentation using L1-regularized NMF was applied to the BRATS 2013 Leaderboard dataset. This has allowed to compare our method directly to the best performing methods from the BRATS 2013 challenge, as well as to several competitive methods from literature. Our semi-automated NMF-based approach outperformed all other methods in terms of mean Dice score for the enhancing tumor region. Competitive results were also found for the tumor core, but relatively low Dice scores were found for the whole tumor region. Incorporating additional prior knowledge should allow further improving segmentation quality, in particular for the whole tumor region, as well as increasing robustness of the segmentation results.

Acknowledgment

This work has been funded by the following projects: Flemish Government FWO (G.0869.12N); IWT IM (n°135005); European Research Council under the European Union's Seventh Framework Programme (FP7/2007-2013): EU MC ITN TRANSACT 2012 (n°316679) and ERC Advanced Grant: BIOTENSORS (n°339804). This paper reflects only the authors' views and the Union is not liable for any use that may be made of the contained information.

References

[1] P. Y. Wen, D. R. Macdonald, D. A. Reardon, T. F. Cloughesy, A. G. Sorensen, E. Galanis, J. DeGroot, W. Wick, M. R. Gilbert, A. B. Lassman *et al.*, "Updated response assessment criteria for high-grade gliomas: response assessment in neuro-oncology working group," *Journal of Clinical Oncology*, vol. 28, no. 11, pp. 1963–1972, 2010.

[2] B. M. Ellingson, T. F. Cloughesy, A. Lai, P. L. Nghiemphu, P. S. Mischel, and W. B. Pope, "Quantitative volumetric analysis of conventional MRI response in recurrent glioblastoma treated with bevacizumab," *Neuro-oncology*, p. noq206, 2011.

[3] M. A. Hammoud, R. Sawaya, W. Shi, P. F. Thall, and N. E. Leeds, "Prognostic significance of preoperative MRI scans in glioblastoma multiforme," *Journal of Neuro-oncology*, vol. 27, no. 1, pp. 65–73, 1996.

[4] Q. T. Ostrom, H. Gittleman, P. Liao, C. Rouse, Y. Chen, J. Dowling *et al.*, "CBTRUS statistical report: primary brain and central nervous system tumors diagnosed in the United States in 2007–2011," *Neuro-oncology*, vol. 16, no. suppl 4, pp. iv1–iv63, 2014.

[5] N. Gordillo, E. Montseny, and P. Sobrevilla, "State of the art survey on MRI brain tumor segmentation," *Magnetic resonance imaging*, vol. 31, no. 8, pp. 1426–1438, 2013.

[6] B. Menze, M. Reyes, K. Van Leemput *et al.*, "The multimodal brain tumor image segmentation benchmark (BRATS)," *IEEE Trans. Med. Imag.*, vol. 34, no. 10, pp. 1993–2024, 2015.

[7] S. Bauer, T. Fejes, J. Slotboom, R. Wiest, L.-P. Nolte, and M. Reyes, "Segmentation of brain tumor images based on integrated hierarchical classification and regularization," in *MICCAI BraTS Workshop. Nice: MICCAI Society*, 2012.

[8] C.-H. Lee, S. Wang, A. Murtha, M. R. Brown, and R. Greiner, "Segmenting brain tumors using pseudo–conditional random fields," in *International Conference on Medical Image Computing and Computer-Assisted Intervention*. Springer, 2008, pp. 359–366.

[9] T. R. Jensen and K. M. Schmainda, "Computer-aided detection of brain tumor invasion using multiparametric MRI," *Journal of Magnetic Resonance Imaging*, vol. 30, no. 3, pp. 481–489, 2009.

[10] L. M. Fletcher-Heath, L. O. Hall, D. B. Goldgof, and F. R. Murtagh, "Automatic segmentation of non-enhancing brain tumors in magnetic resonance images," *Artificial intelligence in medicine*, vol. 21, no. 1, pp. 43–63, 2001.

[11] J. Juan-Albarracín, E. Fuster-Garcia, J. V. Manjón, M. Robles, F. Aparici, L. Martí-Bonmatí *et al.*, "Automated glioblastoma segmentation based on a multiparametric structured unsupervised classification," *PloS One*, vol. 10, no. 5, p. e0125143, 2015.

[12] J. Nie, Z. Xue, T. Liu, G. S. Young, K. Setayesh, L. Guo, and S. T. Wong, "Automated brain tumor segmentation using spatial accuracy-weighted hidden Markov random field," *Computerized Medical Imaging and Graphics*, vol. 33, no. 6, pp. 431–441, 2009.

[13] N. Sauwen, D. M. Sima, S. Van Cauter, J. Veraart, A. Leemans, F. Maes, U. Himmelreich, and S. Van Huffel, "Hierarchical non-negative matrix factorization to characterize brain tumor heterogeneity using multi-parametric MRI," *NMR in Biomedicine*, vol. 28, no. 12, pp. 1599–1624, 2015.

[14] J. G. Sled, A. P. Zijdenbos, and A. C. Evans, "A nonparametric method for automatic correction of intensity nonuniformity in MRI data," *IEEE Trans. Med. Imag.*, vol. 17, no. 1, pp. 87–97, 1998.

[15] N. J. Tustison, B. B. Avants, P. A. Cook, Y. Zheng, A. Egan, P. A. Yushkevich, and J. C. Gee, "N4ITK: improved N3 bias correction," *IEEE Trans. Med. Imag.*, vol. 29, no. 6, pp. 1310–1320, 2010.

[16] N. Vervliet, O. Debals, L. Sorber, M. Van Barel, and L. De Lathauwer, "Tensorlab v3.0 (March 2016)," www.tensorlab.net, [Accessed June-2016].

[17] M. Araújo, T. Saldanha, R. Galvão, T. Yoneyama, H. Chame, and V. Visani, "The successive projections algorithm for variable selection in spectroscopic multicomponent analysis," *Chemometrics and Intelligent Laboratory Systems*, vol. 57, no. 2, pp. 65–73, 2001.

[18] D. Kwon, R. T. Shinohara, H. Akbari, and C. Davatzikos, "Combining generative models for multifocal glioma segmentation and registration," in *MICCAI Conference*. Springer, 2014, pp. 763–770.

[19] G. P. Mazzara, R. P. Velthuizen, J. L. Pearlman, H. M. Greenberg, and H. Wagner, "Brain tumor target volume determination for radiation treatment planning through automated MRI segmentation," *International Journal of Radiation Oncology* Biology* Physics*, vol. 59, no. 1, pp. 300–312, 2004.